JOURNAL OF ENGINEERING SCIENCES

Volume 10, Issue 2 (2023)

Molochkov D., Kulykovskyi R., Brykov M., Hesse O. (2023). The influence of surface irregularities on the mechanical properties of thin-walled wire and arc additively manufactured parts. Journal of Engineering Sciences (Ukraine), Vol. 10(2), pp. A10–A17, doi: 10.21272/jes.2023.10(2).a2

The Influence of Surface Irregularities on the Mechanical Properties of Thin-Walled Wire and Arc Additively Manufactured Parts

Molochkov D.[1*][0000-0002-9030-5371], Kulykovskyi R.[1][0000-0001-8781-2113], Brykov M.[1][0000-0002-8158-1278], Hesse O.[2][0009-0009-9488-5164]

[1] Zaporizhzhia Polytechnic National University, 64, Zhukovsky St., 69063 Zaporizhzhia, Ukraine;
[2] Ernst Abbe University of Applied Sciences Jena, 2, Carl-Zeiß-Promenade St., 07745 Jena, Germany

Article info:
Submitted: June 7, 2023
Received in revised form: September 14, 2023
Accepted for publication: September 21, 2023
Available online: September 22, 2023

***Corresponding email:**
dmolochkov@gmail.com

Abstract. Wire and Arc Additive Manufacturing (WAAM) is a metal additive manufacturing process commonly used to deposition medium to large, near net-shaped parts. It can efficiently use materials and deposit objects with fewer assembly parts. The main disadvantage of WAAM is the surface quality. This work investigates the geometry shift defect that could be formed due to the wear of the welding contact tip. As a result of the wear, the filler wire deviates from the nominal position, and errors occur in the positioning of individual layers of printed parts. The main objective of this work is to investigate the influence of surface irregularities on the mechanical properties of as-deposited thin-walled WAAM parts. Finite element modeling of static and cyclic tensile and compressive tests showed that the surface waviness formed during layer-by-layer deposition increases the stress level under static loading applied transversely to the deposited layers. Surface waviness also significantly reduces the life of parts under cyclic loading. Replacement of a worn contact tip causes the layers to shift, and the resulting load eccentricity increases the stress level. Uneven stress distribution throughout the cross section means reduced material usage efficiency. During compressive loading, the load eccentricity destabilizes, causing the specimen to deform after exceeding the yield strength in stress concentration zones. The relationship between unmachined and machined walls with equivalent stresses was obtained, allowing the influence of surface waviness on the strength and durability of structures to be considered at the design stage.

Keywords: additive manufacturing, process innovation, geometry defect, stress concentrator, fatigue strength.

1 Introduction

Additive technologies, such as Wire and Arc Additive Manufacturing (WAAM), offer the benefits of reducing material consumption and shortening production time for single parts or small batches. However, one downside of layer-by-layer manufacturing is the unevenness of the surfaces it produces. While other manufacturing methods like milling or powder fusion result in surface roughness ranging from 0.63 to 2.5 μm and 16 to 18 μm, respectively, WAAM can generate surfaces with a waviness of 0.15 to 1.0 mm [1, 2].

WAAM utilizes gas metal arc welding, gas tungsten arc welding, or plasma arc welding to deposit metal layers and create three-dimensional structures. The accuracy of wire positioning during the deposition process is crucial for achieving precise results. However, fluctuations of the filler wire caused by its curvature and wearing of welding torch parts contribute to the increased surface waviness of the printed parts and can cause defects in their geometry.

Despite the relatively low surface quality, unmachined WAAM parts have the potential to be used in a wide range of industries. For example, a 3D-printed gearbox housing part may only need to be machined with other parts or assemblies at the contact surfaces. Reducing the amount of finishing required on the printed parts will positively impact production time and associated machining costs.

This article aims to analyze the effect of surface irregularities and defects in part geometry on the mechanical properties of unmachined thin-walled WAAM parts.

2 Literature Review

Minimizing the amount of machining in the production of medium and large parts (e.g., gas turbine casings, gearbox housings, and reinforced concrete elements) will speed up production and reduce the consumption of cutting tools and electricity, as well as the number of production steps. However, the design and use of parts "as deposited", i.e., in raw form, can have their peculiarities due to the typical WAAM surface quality and possible geometric defects.

However, the typical surface waviness of the WAAM part geometry resulting from layer-by-layer deposition and metal crystallization, as well as metal deposition defects (e.g., different bead wetting angles, metal run-off, and bead intersections), potentially affect the mechanical properties of the parts and should therefore be considered in the analysis and design of structures [3]. In addition to material microstructure, surface irregularities are another source of anisotropy in mechanical properties. Tensile and compression test results for unmachined stainless steel specimens show a 10 % lower tensile strength and $\sigma_{0.2}$ yield strength when loaded transversely to the deposited layers than specimens loaded longitudinally to the layers. In addition, a reduction in Young's modulus of up to 20 % has been observed for transverse specimens [4, 5].

One of the main reasons for the variation in mechanical properties in different orientations is the unequal effective cross-sectional area of the part or specimen when loaded longitudinally and transversely to the deposited layers [6]. The effective cross-sectional area or effective wall width (EWW) is the size parameter of the wall cross-section that can be effectively used after the total wall width (TWW) has been machined [7]. The TWW is the sum of the EWW, the surface waviness on both sides, and the additional machining allowance, if any.

Other studies have also investigated the mechanical properties of machined and unmachined ER308LSi stainless steel specimens. In the longitudinal direction, both specimens show similar results, i.e., surface irregularities do not significantly affect the mechanical properties. However, in the transverse direction to the layers, the yield strength and strain of the unmachined specimens are almost 10 and 20% lower, respectively, than those of the machined specimens of equivalent effective wall width [8, 9].

In addition to the typical waviness, WAAM can produce geometric deviations independent of the deposition parameters but related to contact tip wear. The contact tip is an element of the welding torch that guides the filler wire to the welding location and through which the electric current is transmitted to the wire (Figure 1 a). Due to the constant movement of the wire at a speed of 3–15 m/min, mechanical wear occurs in which the contact tip with lower hardness (the hardness of the CuCrZr alloy tip according to various data is 155 HB [10] and 150 HV [11]) interacts with the more rigid wire (Inconel 718 hardness in the range of 250–300 HV [12]; low-carbon wire ER70S-6 in the range of 140–170 HV [13–15]).

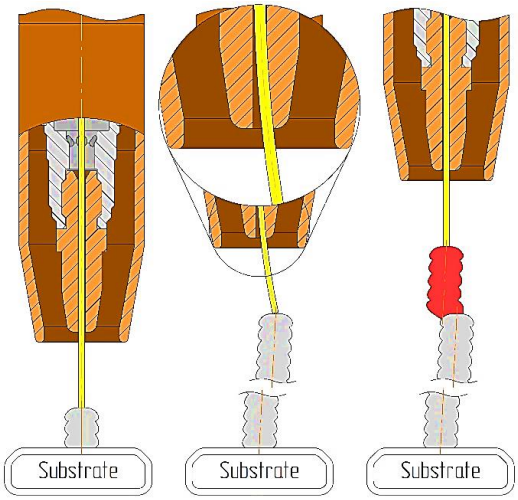

Figure 1 – Schematic representation of filler wire deviation: a – the contact tip; b – changes in the relative position of the wire; c – replaced tip

Wear of the contact tip will naturally lead to changes in the relative position of the wire, which directly affects the stability and accuracy of the material deposition (Figure 1 b). Over time, a worn tip will need to be replaced due to excessive deviation of the wire from the programmed path or because the wire sticks to the tip due to high transient resistance or spatter. Replacing a worn tip with a new one is also followed by a change in the relative position of the wire to its original position (Figure 1 c). Thus, the relative change in wire position will constantly accompany the deposition process, causing the geometric parameters to deviate from the acceptable range.

Surface waviness is one of the factors that reduces the mechanical properties of 3D-printed objects. In order to achieve the required level of mechanical properties, it is therefore necessary to either machine or increase the wall width. Machining is not always possible in the case of complex product shapes or large dimensions, so compensating for the reduction in mechanical properties of parts by increasing the wall width of parts is an effective method.

In order to promote the use of unmachined parts in various industries and to increase the wall width by a reasonable amount, it is necessary to determine the ratio of unmachined and machined wall width of parts that will experience the same stresses under equal loads.

At the same time, it is necessary to investigate the effect of the shape displacement defect formed by the worn tip replacement on the mechanical properties of unmachined specimens.

3 Research Methodology

Changing the position of the filler wire concerning the torch during the wear of the contact tip or after replacing it with a new one often leads to the formation of a defect that looks like a parallel displacement of the part element in the direction of the filler wire deviation.

Three groups of specimens (A, B, and C) were printed (Figure 2) to investigate the effect of geometry distortion on the mechanical properties of thin-walled parts.

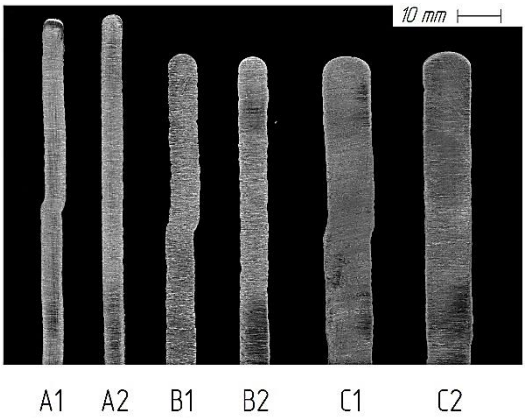

Figure 2 – Scans of 3D-printed specimens

Each group consisted of two specimens and differed in wall width. Specimens A1, B1, and C1 had a geometry defect caused by a shift in the deposition path. Specimens A2, B2, and C2 were printed using the same WAAM parameters without reproducing the defect.

The main filler material was Lincoln Electric ER70S-6 1.2mm low-carbon welding wire, deposited using Cold Metal Transfer (CMT) technology. The welding equipment used was a Yaskawa MA 1440 welding robot, a Fronius TPS 500i power source with two wire feeders, and a CMT option. The main deposition parameters and material properties are summarised in Tables 1 and 2.

Table 1 – Main deposition parameters

Travel speed, cm/min	Wire feed, m/min	Average amperage, A	Average voltage, V	Gas rate, l/min	Working distance, mm
45	2.8	107	13.1	14 ± 1	15 ± 0.5

Table 2 – Mechanical properties of the material [16]

Ultimate strength, Pa	Yield strength, Pa	Young's modulus, Pa	Poisson's ratio
$5.54 \cdot 10^8$	$4.1 \cdot 10^8$	$1.98 \cdot 10^{11}$	0.3
Tangential modulus, Pa	Bulk modulus, Pa	Shear modulus, Pa	Density, kg/m^3
$1.45 \cdot 10^9$	$1.65 \cdot 10^{11}$	$7.6154 \cdot 10^{10}$	7850

The trajectory direction was reversed for each layer to compensate for the difference in height at the beginning and the end of the beads.

In the study, it was assumed that the material structure was the same for all specimens; therefore, the geometric parameters of the specimens determined their mechanical properties.

The research in this paper was based on finite element modeling of mechanical testing of printed specimens using ANSYS Mechanical software. Using simulation tools allowed the geometric imperfections of the printed parts to be modeled and the actual non-linear behavior of stresses and strains to be investigated so that all potential failure modes could be considered in the design. Such digital twins, together with the properties of the deposited materials known from experimental studies, allowed analytical testing under different types of loading and the study of complex non-linear phenomena

3D simulation models were created based on 2D optical scanning of the specimens' cross-sections (Figure 3).

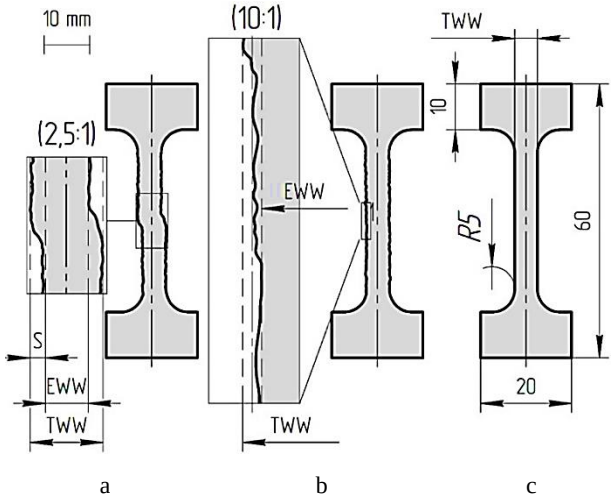

Figure 3 – Geometry of the specimens: a – specimen with geometry displacement defect; b – specimen without displacement defect; c – reference specimen

The images obtained have a density of 1200 pixels/inch, or 47 244 px/mm, which allowed a detailed profile of the specimen models to be created.

The study involved taking central parts of 40 mm high and 20 mm long specimens. Layers in these specimens had an average height of 1.40 mm. The geometric parameters of these specimens are provided in Table 3.

Table 3 – Numerical geometry parameters of 3D printed specimens

Specimen	TWW, mm	EWW, mm	Waviness, mm	Defect size, mm	Tensile loading, kN	Compression loading, kN
A1	6.41	3.77	1.32	1.06	19.9	19.2
A2	5.61	4.79	0.41	–		
A3	4.79	4.79	0.00	–		
B1	8.29	4.81	1.74	1.25	21.5	21.4
B2	7.01	5.89	0.56	–		
B3	5.89	5.89	0.00	–		
C1	12.46	9.38	1.54	1.26	39.0	38.9
C2	11.41	10.41	0.50	–		
C3	10.41	10.41	0.00	–		

The displacement S of the wire used in the deposition process was measured to be 1.15 ± 0.05 mm, indicating the deflection after 1350 ± 50 m (2.8 ± 0.1 kg) deposited filler wire (Figure 3 a). This displacement resulted in corresponding deviations in specimens A1, B1, and C1 (Table 3). Comparisons were then made between these printed specimens and reference specimens A3, B3, and C3 (Figure 3 c) with machined geometry (specimens A2, B2, and C2 machined to EWW) (Table 3). The study aimed to determine the impact of irregularities and geometry defects on the mechanical properties.

To simplify the analysis, it was assumed that the cross-sectional shape remained constant throughout the length of the specimens. Under this assumption, simulations were conducted in one plane, and analytical results were obtained for three-dimensional models with a length of 20 mm. The profile of each specimen was divided into quadrilateral elements with a grid spacing of 0.2 mm.

Typically, parts in different structures are subjected to static and dynamic loads. The main example of static loads in different structures is their weight. It acts with a constant force or changes over a long time. A static tensile test allows the strength of a specimen to be determined under a one-time load, while cyclic loading allows the fatigue failure of a specimen to be studied.

The models of the printed specimens were tested under uniaxial tensile and compressive static loads of 19.9, 21.5, and 39.0 kN, respectively, for groups A, B, and C. The selected load values were chosen as a result of preliminary modeling. They correspond to the maximum safe loads for unmachined specimens without defects (A2, B2, C2), at which the specimens' stresses will equal the yield strength.

The specimens were also subjected to a pulsating cyclic load with a specific force and complete unloading to simulate their use in various applications such as lifting mechanisms, structures, pressure vessels, bridges, buildings, and vehicles. The maximum σ_{max} and minimum σ_{min} stresses experienced during asymmetric cycles were unequal. Hence, the influence of average stresses Δσ on specimen damage had to be considered (Figure 4).

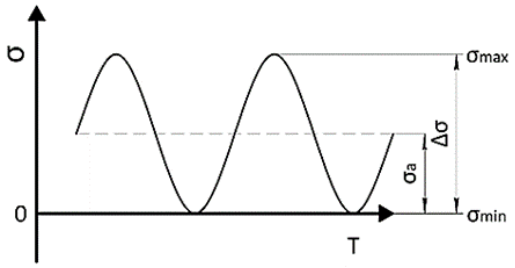

Figure 4 – Cyclic loading schematic diagram

The analysis utilized the Δσ correction method based on the Soderberg diagram, a traditional yield strength method, to estimate fatigue limit. Structural steel's fatigue limit for different loading cycles was sourced from the ANSYS material library (Table 4).

Table 4 – Yield strength of material used

Number of cycles	$1 \cdot 10^1$	$2 \cdot 10^1$	$5 \cdot 10^1$	$1 \cdot 10^2$	$2 \cdot 10^2$	$1 \cdot 10^3$	$1 \cdot 10^4$	$2 \cdot 10^4$	$1 \cdot 10^5$	$2 \cdot 10^5$	$1 \cdot 10^6$
Cyclic stresses, MPa	3999	2827	1896	1413	1069	441	262	214	138	114	86.2

4 Results

4.1 Tensile simulation analysis

Tensile modeling of the printed specimens was carried out using the finite element method to determine the maximum stresses and strain of the specimens under static tensile loading. The maximum number of cycles the specimens could withstand under the same loading parameters was also determined.

The simulation of a tensile test under uniaxial longitudinal loading of the printed specimens transverse to the deposited layers showed the effect of surface irregularities and other geometric defects on the stress distribution in the part (Figure 5 a). The pits formed between the layers were stress concentrators, which became the zones of onset of plastic deformation and fracture of the parts. At a load of 19.9 kN, the maximum stresses in the body of the A2 specimen were 410 MPa, corresponding to the yield strength of the material used (Figure 5 a). At the same time, the strain did not exceed 0.2 %, and there was no residual deformation.

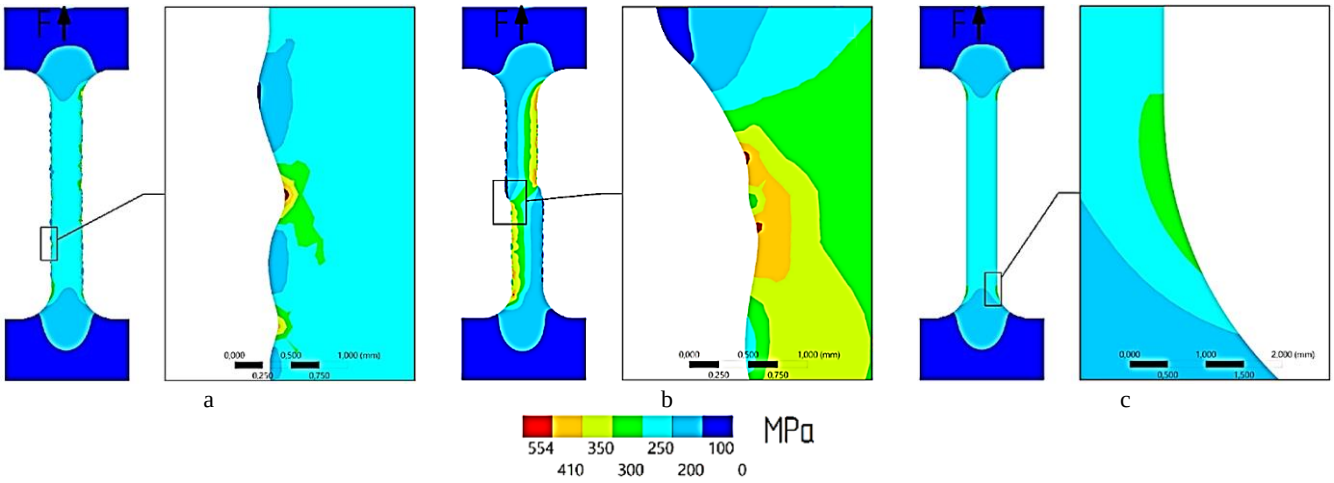

Figure 5 – Stress distribution during tensile test: a – without defects; b – with displacement defect; c – reference specimen

The maximum stresses in specimen A1 reached 430 MPa, which exceeded the yield strength by 4.9 % and caused plastic deformation (Figure 5 b). The highest stresses were concentrated in the geometry displacement areas of the specimen and near-surface zones located around the pits between the deposited metal layers. It should be mentioned that the crack resistance varied among different materials, resulting in varying responses to stress concentrators. In addition to the maximum stresses, it is necessary to pay attention to the stresses in the range of 300–410 MPa, which were located along the surfaces closest to the central axis of the cross-section. The uneven stress distribution in specimen A1 was primarily due to the position of the upper and lower halves of the specimen. During tensile testing, a tangential stress component and an additional force moment were generated in the defect zone due to the eccentric load, leading to higher stresses than specimens without defects. In the specimen with displacement, the strain is 0.51 %, and the residual deformation is 0.29 %.

The uneven stress distribution along the cross-section of specimen A1 and the non-optimal use of this material under the specified load was confirmed by the value below 200 MPa near the surface of the protruding elements (Figure 5 b). In specimen A2 (Figure 5 a), the total stresses were 200–300 MPa under similar loading conditions, and their distribution is more uniform along the cross-section.

The maximum stresses in reference specimen A3 during tensile testing were 262 MPa (Figure 5 c). Simultaneously, the maximum stress concentration was observed in the transition zones from the tested wall to the gripping edges at a depth of up to 0.1 mm. From a depth of 0.75 mm, the stresses were 200–205 MPa.

Group B and C specimens showed similar stress distribution across the cross-section. In specimens B1 and C1, the concentration of high stresses was observed in several transition zones from one layer to another, indicating that plastic deformation was taking place at this location. The highest stresses in specimen B1 during tensile testing reached 442 MPa, which is 7.8 % more than the yield strength of the material. At a depth of 0.1 mm from the specimen's surface, the stress level decreased to 350–360 MPa, and at a depth of 0.5–1.0 mm – to 250–275 MPa. Along the center line of the specimen B1, the stresses did not exceed 170–180 MPa. The strain under load was 0.38 %, and residual deformations were 0.16 %.

The stresses in specimen C1 reached 453 MPa at the previously indicated locations, i.e., 10.5 % more than the safe level, and decreased to 255 MPa at a depth of 0.7 mm. In the center of the specimen body, in the displacement zone, the stresses decreased to 190 MPa. Under load, the strain is 0.25 %, and the residual strain is less than 0.02 %.

When the corresponding loads were applied, the specimens with no displacement defects B2 and C2 had maximum stresses at the yield strength level (Table 3). As in the previous specimens, these stresses were concentrated near the wall's surface around the transition pits between the layers to a depth of 0.25 mm. Unlike the specimens with defects, the stresses in specimens B2 and C2 were more evenly distributed across the width and did not exceed 180 MPa from a depth of 0.75–1.00 mm. The strain of both specimens under load did not exceed 0.2 %, and there were no residual deformations.

The stresses in reference specimens B3 and C3 were distributed similarly to specimen A3, with maximum values at the rounded transition zones of 242 MPa for B3 and 301 MPa for C3. From a depth of 0.5–0.9 mm, the stresses decreased to 215 MPa; in the center of the specimens' bodies, the stresses did not exceed 190 MPa.

Undoubtedly, the presence of many stress concentrators would reduce the tensile strength of the parts under static loading, but the surface's unevenness would have a more significant effect on the fatigue strength of the parts. Machine parts often operate under variable loads and can fail at stresses below the tensile or yield strength. The ability of a material to withstand cyclic loading is called fatigue strength, which its fatigue limit could describe. The magnitude of the fatigue limit of materials depends on the structure of the material, the manufacturing and processing technology, the working temperature, the surface quality and related stress concentration, and the loading mode. Therefore, to exclude fatigue destruction of machine parts and structures, the fatigue limit should be determined experimentally for each operating condition [17].

The cyclic loading simulation showed that the reference A3 specimen's life under the specified conditions was 31476 stress cycles, after which its destruction began (Figure 5 c). At the same time, the A2 specimen started to collapse after 2618 cycles, which was more than 12 times less than the reference specimen. In this case, the destruction's origins were the stress concentrators in the near-surface zones of the material formed by the typical surface waviness (Figure 5 a). The defect in specimen A1 reduced the fatigue life to 1921 cycles.

Group B and C specimens had fairly close fatigue life values. The reference specimens B3 and C3 withstanded 49 500 and 14 200 cycles before failure occurred. The surface waviness of specimens B2 and C2 reduced the life to 2715 and 2622 cycles, and the displacement defect in specimens B1 and C1 worsened the situation to 1745 and 1574 cycles, respectively.

Typically, engineering calculations of safety loads consider their part's operation at stresses not exceeding the yield strength. Exceeding means irreversible plastic deformation will occur, resulting in loss of shape and strength of the part after unloading. Thus, exceeding the yield strength in the specimens with displacement (Figure 5 b) indicated that plastic deformation occurred in the first cycle, and therefore, its shape was distorted, which is unacceptable in regular operation.

4.2 Compression simulation analysis

Compression test simulations were carried out to determine the effect of surface irregularities in the 3D-printed thin-walled parts on their behavior under compressive loading. In a compression test, the key parameter for analysis was the maximum force achieved before the specimen broke or deformed.

The static load in Table 3, applied in the vertical direction, showed the negative effect of the geometry displacement of specimens A1, B1, and C1 on the stability

of the structure. In compression and tension, the stresses in the specimens with displacement were distributed asymmetrically with respect to the axis of load application along their cross-section (Figure 6).

The highest stresses of 437 MPa in specimen A1 were concentrated around the transition pit between the layers. At a depth of 0.5 mm, the stresses decreased to 315 MPa. In the specimen cross-section below the defect, the stresses varied from 380...430 MPa on the one hand to 40...50 MPa on the other and vice versa above the defect. Exceeding the yield strength with a similar stress distribution in the near-surface zones resulted in the bending of the specimen and destabilization of the structure.

The maximum stresses of 448 and 461 MPa in specimens B1 and C1, respectively, were also related to the waviness of the surfaces. At a depth of 0.50–0.75 mm, the stresses decreased to 275–300 MPa, and in the center of the specimens in the deformation zone to 185–190 MPa. Similar to A1, the stresses were asymmetrically distributed on different sides of the specimens (Figure 6 b).

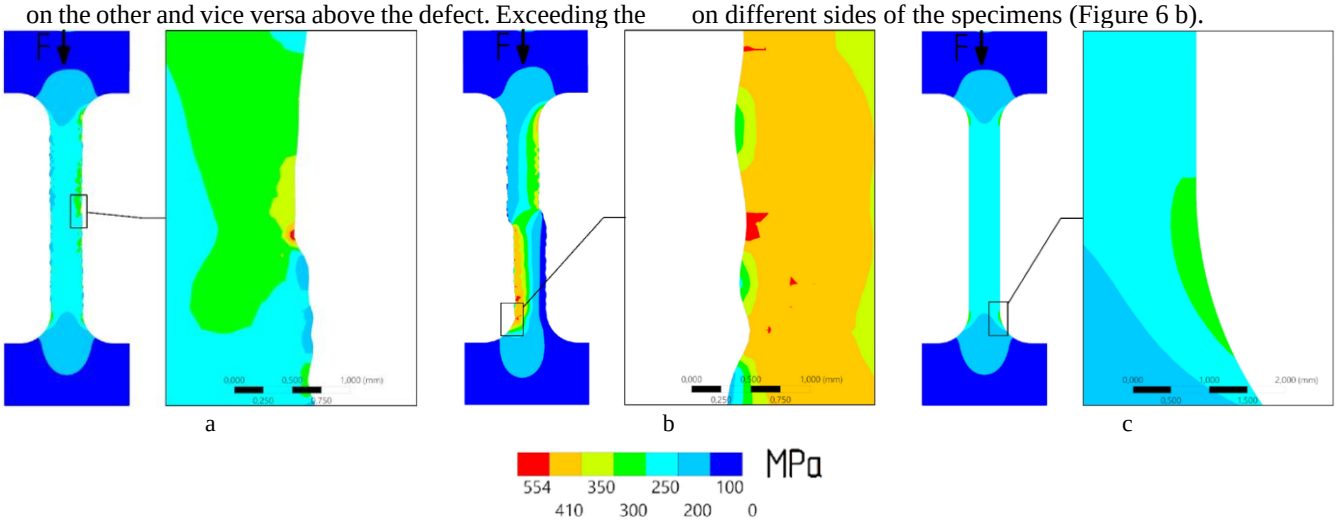

Figure 6 – Stress distribution during compression test: a – without defects; b – with displacement defect; c – reference specimen

Exceeding the yield strength in compression of the specimens with displacement indicated the presence of plastic deformation. Specimens A1, B1, and C1 strain was 0.67, 0.36, and 0.25 %, respectively, beyond the elastic deformation limit. The residual deformations were 0.45, 0.14, and 0.02 %, respectively.

Specimens A2, B2, and C2 at the corresponding loads (Table 3) showed the highest stresses equal to the yield strength, concentrated around the transition pits between the layers. Simultaneously, stresses in the 300–400 MPa range were concentrated only near one of the surfaces of the specimens.

At a depth of 0.15–0.5 mm, the stresses decreased to 250 MPa; at a depth of 0.5–2.0 mm, they were at 170–200 MPa. These stresses were located on one of the wall surfaces, while on the other side, at a depth of 0.15 mm, they were in the 170–180 MPa range. An uneven stress distribution can lead to the bending of the specimen when the load is increased.

In reference specimens A3, B3, and C3, under the same loading conditions, the maximum stresses did not exceed 250–300 MPa (Figure 6 c). Due to the symmetry of the specimens and the absence of waviness of the side surfaces, the stresses were distributed evenly throughout the cross-section, and their value in the main body of the walls did not exceed 180 MPa.

Thus, the formed defect significantly shifted the stress distribution in the specimens under compression, degrading the stability of the structures and increasing the maximum stresses, leading to their deformation. The strain of the specimens without displacement defect and the reference specimens did not exceed 0.2 %, and there were no residual deformations.

It was also found that under cyclic loading, specimens A1, B1, and C1 could withstand up to 1809, 1649, and 1467 cycles, respectively, before failure occurred at critical locations in the near-surface zones at a depth of up to 0.25 mm between deposited layers (Figure 6 b).

Fracture initiation under cyclic loading of specimens A2 – 2628 cycles, A3 – 38 822 cycles, B2 – 2637 cycles, B3 – 50 796 cycles, C2 – 2629 cycles, and C3 – 14 418 cycles.

For the displacement defect specimens, plastic deformation occurred during the first load cycle due to exceeding the tensile strength, i.e., the decrease in fatigue life under cyclic loading is critical compared to the other specimens (Figure 6 b).

5 Discussion

The results showed a reduction in the mechanical properties of the specimens due to the presence of stress concentrators formed by surface irregularities. The resulting stresses reduced the effective wall width, which increased the chances of premature failure due to non-optimal stress distribution across the part.

The example of the 3D printed specimens A2, B2, and C2 shows that the typical waviness of the WAAM specimen surfaces without displacement defect increases the maximum stresses by 37–69 %, and the displacement defect in the specimen geometry increases the stresses by 51–80 % compared to the reference specimens.

As a result, unmachined specimens have a higher risk of fracture or plastic deformation when subjected to loads

close to the safe limit. Given that, in some cases, traditional methods of mechanical processing may not be available (e.g., large dimensions of the printed objects and depositing on site), it is necessary to ensure the reliability of the structures by reducing the calculated safe loads, i.e., reducing the stress level by increasing the wall width.

Based on the analysis, an equivalent wall width (EqWW) has been determined for each printed specimen. EqWW describes the width of a machined specimen with the same stress level as the printed specimen under specified loads (Table 5).

Mechanical stresses at a point in a body are defined as a vector of internal forces acting on a unit area:

$$\sigma = \frac{F}{A}, \quad (1)$$

where σ – normal stress, Pa; F – applied load, N; A – cross-sectional area, m^2.

Table 5 – Machined wall width with equivalent stresses

Specimen	Load, kN	Maximum stresses, MPa	EqWW, mm
A1	19.9	430	2.35
A2		410	2.60
B1	21.5	442	2.50
B2		409	3.05
C1	39.0	453	4.50
C2		410	5.00

Using this formula, a preliminary equivalent cross-sectional area has been determined and verified by simulation in ANSYS Mechanical.

The established relationship between EqWW and TWW is linear, which may indicate a proportional effect of surface waviness on stresses at different TWW (Figure 7).

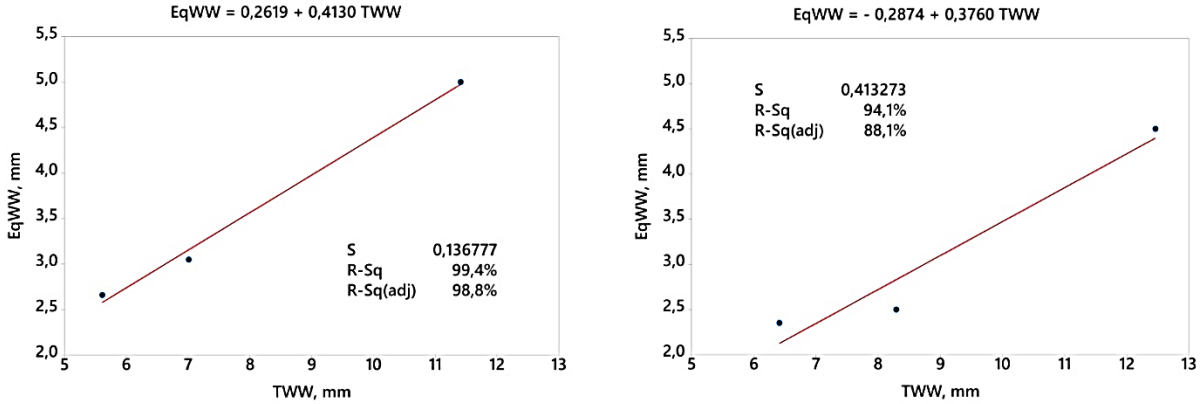

Figure 7 – Relationship between unmachined and machined walls width: a – without defects; b – with displacement effect

6 Conclusions

This paper presents the research results on the influence of surface irregularities in WAAM parts on their mechanical properties. When using 3D printed objects without machining or other methods of improving the surface quality, it is first necessary to consider the geometric deviations that occur due to disturbances in the deposition process and that can affect the strength of the structure and its functionality. Three groups of specimens printed under the same conditions have been used to simulate the effect of a defect created after replacing a worn contact tip. Firstly, the shift in part geometry increases the positioning error of individual printed elements, resulting in uneven stress distribution under compressive and tensile loads.

The defect resulting from replacing the contact tip significantly changes the nature of the stress distribution in the tensile specimens, increasing the maximum stresses by 4.9–10.5 % relative to the specimens without the displacement defect.

Tensile testing of unmachined specimens with no displacement defect shows that surface waviness increases the stress concentration in the near-surface zones up to a depth of 0.25–0.50 mm. These concentrators are particularly critical under cyclic loading, as they become zones of crack initiation, and the onset of fracture is up to 20 times faster.

At the same time, specimens with a defect formed after replacing a worn contact tip with a new one show an additional reduction in mechanical properties due to the formation of a load eccentricity. In tension, such a defect is an additional stress concentrator; in compression, the structures lose stability more quickly.

It has been found that defects formed due to contact tip wear during WAAM of thin-walled parts have a critical effect on the strength and durability of the structure. Since structural elements are usually designed to operate under load conditions not exceeding the yield strength or to meet a particular stiffness requirement, the uncontrolled occurrence of such defects is unacceptable.

The paper established the relationship between unmachined and machined wall width at equivalent stresses. The resulting relationship makes it possible to consider the influence of surface waviness on the strength and durability of structures at the design stage and to compensate for the waviness of the parts' surfaces and the additional stresses it generates by increasing the total wall width (TWW) by a certain amount. In this way, it is possible to compensate for the reduction in the mechanical properties of the parts and to reduce the number of stages in the technological process of their manufacture by reducing the need for machining.

Regardless of the solution found, avoiding a possible reduction in fatigue life by increasing the size of structural elements reduces the efficiency of material use. In addition, the effect of the geometry displacement defect should be investigated for each component, which has a specific design and individual working conditions.

Contact tip wear is an irreversible and gradual process that changes the relative position of the filler wire and, consequently, the location of the material deposition. By studying the wear rate of the contact tip under different deposition process parameters, optimizing its replacement's periodicity and predicting the wire's relative deviation when creating the deposition trajectory will be possible. Reducing the size and number of geometric defects will help to reduce the amount of post-processing required, making production faster and cheaper.

It should be noted that the above results refer to printed specimens produced under a specific set of parameters.

Further research will generalize these results to investigate the effect of geometric irregularities and defects on the mechanical properties of GMAW-based WAAM parts.

References

1. Fonseca, P. P., Vidal, C., Ferreira, F., Duarte, V. R., Rodrigues, T. A., Santos, T. G., Machado, C. M. (2022). Orthogonal cutting of Wire and Arc Additive *Manufactured parts. The International Journal of Advanced Manufacturing Technology*, Vol. 119(7–8), pp. 4439–4459. https://doi.org/10.1007/s00170-022-08678-3
2. Martina, F., Mehnen, J., Williams, S. W., Colegrove, P., Wang, F. (2012). Investigation of the benefits of plasma deposition for the additive layer manufacture of Ti–6Al–4V. *Journal of Materials Processing Technology*, Vol. 212(6), pp. 1377–1386. https://doi.org/10.1016/j.jmatprotec.2012.02.002
3. Laghi, V., Palermo, M., Gasparini, G., Girelli V. A., Trombetti, T. (2019). Geometrical characterization of wire-and-arc additive manufactured steel element. *Advanced Materials Letters*, Vol. 10(10), pp. 695–699. https://doi.org/10.5185/amlett.2019.0019
4. Laghi, V., Palermo, M., Gasparini, G., Girelli, V. A., Trombetti, T. (2020). Experimental results for structural design of wire-and-arc additive manufactured stainless steel members. *Journal of Constructional Steel Research*, Vol. 167, 105858. https://doi.org/10.1016/j.jcsr.2019.105858
5. Hadjipantelis, N., Weber, B., Buchanan, C., Gardner, L. (2022). Description of anisotropic material response of wire and arc additively manufactured thin-walled stainless steel elements. *Thin-Walled Structures*, Vol. 171, 108634. https://doi.org/10.1016/j.tws.2021.108634
6. Kyvelou, P., Slack, H., Mountanou, D. D., Wadee, M. A., Britton, T. B., Buchanan, C., Gardner, L. (2020). Mechanical and microstructural testing of wire and arc additively manufactured sheet material. *Materials and Design*, Vol. 192, 108675. https://doi.org/10.1016/j.matdes.2020.108675
7. Chernovol, N., Sharma, A., Tjahjowidodo, T., Lauwers, B., Van, R. P. (2021). Machinability of wire and arc additive manufactured components. *CIRP Journal of Manufacturing Science and Technology*, Vol. 35, pp. 379–389. https://doi.org/10.1016/j.cirpj.2021.06.022
8. Laghi, V., Palermo, M., Gasparini, G., Girelli, V. A., Trombetti, T. (2021). On the influence of the geometrical irregularities in the mechanical response of wire-and-arc additively manufactured planar elements. *Journal of Constructional Steel Research*, Vol. 178, 106490. https://doi.org/10.1016/j.jcsr.2020.106490
9. Laghi, V., Palermo, M., Silvestri, S., Gasparini, G., Trombetti, T. (2021). Experimental behaviour of wire-and-arc additively manufactured stainless steel rods. *CE/Papers*, Vol. 4(2–4), pp. 2387–2392. https://doi.org/10.1002/cepa.1565
10. Zhang, X., Yuan, Y., Zhao, S., Zhang, J., Yan, Q. (2022). Microstructure stability, softening temperature and strengthening mechanism of pure copper, CuCrZr and Cu-Al_2O_3 up to 1000 °C. *Nuclear Materials and Energy*, Vol. 30, 101123. https://doi.org/10.1016/j.nme.2022.101123
11. Kulczyk, M., Pachla, W., Godek, J., Smalc-Koziorowska, J., Skiba, J., Przybysz, S., Wróblewska, M., Przybysz, M. (2018). Improved compromise between the electrical conductivity and hardness of the thermo-mechanically treated CuCrZr alloy. *Materials Science and Engineering: A*, Vol. 724, pp. 45–52. https://doi.org/10.1016/j.msea.2018.03.004
12. Van, D., Dinda, G. P., Park, J., Mazumder, J., Lee, S. H. (2020). Enhancing hardness of Inconel 718 deposits using the aging effects of cold metal transfer-based additive manufacturing. *Materials Science and Engineering A*, Vol. 776, 139005. https://doi.org/10.1016/j.msea.2020.139005
13. Ermakova, A., Mehmanparast, A., Ganguly, S., Razavi, J., Berto, F. (2020). Investigation of mechanical and fracture properties of wire and arc additively manufactured low carbon steel components. *Theoretical and Applied Fracture Mechanics*, Vol. 109, 102685. https://doi.org/10.1016/j.tafmec.2020.102685
14. Aldalur, E., Veiga, F., Suárez, A., Bilbao, J., Lamikiz, A. (2020). High deposition wire arc additive manufacturing of mild steel: Strategies and heat input effect on microstructure and mechanical properties. *Journal of Manufacturing Processes*, Vol. 58, pp. 615–626. https://doi.org/10.1016/j.jmapro.2020.08.060
15. Nemani, A. V., Ghaffari, M., Nasiri, A. (2020). Comparison of microstructural characteristics and mechanical properties of shipbuilding steel plates fabricated by conventional rolling versus wire arc additive manufacturing. *Additive Manufacturing*, Vol. 32, 101086. https://doi.org/10.1016/j.addma.2020.101086
16. Müller, J., Grabowski, M., Müller, C., Hensel, J., Unglaub, J., Thiele, K., Kloft, H., Dilger, K. (2019). Design and parameter identification of wire and arc additively manufactured (WAAM) steel bars for use in construction. *Metals*, Vol. 9(7), 725. https://doi.org/10.3390/met9070725
17. Pedersen, M. M. (2018). *Introduction to Metal Fatigue – Concepts and Engineering Approaches*. Aarhus University, Aarhus, Denmark. Available online: https://doi.org/10.13140/RG.2.2.25216.28163